

Review

Development of Positron-Emission Tomography/Single-Photon Emission Computed Tomography Imaging Probes for *in Vivo* Detection of β -Amyloid Plaques in Alzheimer's Brains

Masahiro ONO

Department of Patho-Functional Bioanalyses, Graduate School of Pharmaceutical Sciences, Kyoto University; 46–29 Yoshida Shimoadachi-cho, Sakyo-ku, Kyoto 606–8501, Japan.

Received May 29, 2009

Currently, the development of radiotracers for *in vivo* imaging of β -amyloid plaques in Alzheimer's disease (AD) brains is an important, active area of molecular imaging. Postmortem brains of AD patients reveal neuropathologic features: the presence of β -amyloid plaques and neurofibrillary tangles, which contain β -amyloid peptides and highly phosphorylated tau proteins. Increases in the concentration of β -amyloid in the course of the disease lead to changes in AD brains. Thus, when used in combination with positron-emission tomography/single-photon emission computed tomography (PET/SPECT), β -amyloid imaging agents could serve as surrogate markers for the early diagnosis and neuropathogenetic studies of AD. Furthermore, quantitative evaluation of β -amyloid plaques in the brain could facilitate the evaluation of the efficacy of anti-amyloid therapies that are currently being investigated. This paper reviews our research on the development of PET/SPECT imaging agents for *in vivo* detection of β -amyloid plaques in Alzheimer's brains.

Key words molecular imaging; Alzheimer's disease; β -amyloid; positron-emission tomography/single-photon emission computed tomography

Introduction

Alzheimer's disease (AD) is a neurodegenerative disease of the brain associated with irreversible cognitive decline, memory impairment, and behavioral changes. Postmortem brains of AD patients reveal neuropathologic features: the presence of senile plaques (SPs) and neurofibrillary tangles (NFTs), which contain β -amyloid ($A\beta$) peptides and highly phosphorylated tau proteins.^{1,2)} Although the precise mechanism of neuronal death in AD is still unknown, it is widely accepted that SPs and NFTs play a central role in its development. Currently, the only definitive confirmation of AD is by postmortem histopathologic examination of $A\beta$ deposits in the brain. Therefore $A\beta$ plaques in the brain may be useful as a biomarker for the differential diagnosis of AD, and the detection of individual $A\beta$ plaques *in vivo* by positron-emission tomography (PET) or single-photon emission computed tomography (SPECT) should improve diagnosis and also accelerate discovery of effective therapeutic agents for AD.^{3,4)} A number of groups have worked to develop PET/SPECT imaging probes including [¹¹C]-2-4'-(methylaminophenyl)-6-hydroxybenzothiazole ([¹¹C]PIB),^{5–8)} [¹¹C]-4-*N*-methylamino-4'-hydroxystilbene ([¹¹C]SB-13),^{9,10)} [¹⁸F]-4-(*N*-methylamino)-4'-(2-(2-(2-fluoroethoxy)ethoxy)ethoxy)stilbene ([¹⁸F]BAY94-9172),^{11,12)} [¹¹C]-2-(2-(2-dimethylaminothiazol-5-yl)ethenyl)-6-(2-(2-fluoroethoxy)benzoxazole ([¹¹C]BF-227),¹³⁾ [¹⁸F]-2-(1-(2-(*N*-(2-fluoroethyl)-*N*-methyl-

amino)naphthalene-6-yl)ethylidene)malononitrile ([¹⁸F]-FDDNP),^{14–17)} and [¹²³I]-6-iodo-2-(4'-dimethylamino)phenyl-imidazo[1,2-*a*]pyridine ([¹²³I]IMPY)^{18–21)} (Fig. 1). This paper reviews research on the development of PET/SPECT imaging agents for the *in vivo* detection of $A\beta$ plaques in Alzheimer's brains.

PET Probes for Imaging of $A\beta$ Plaques Derived from Stilbene and Benzofuran

As part of efforts to develop ¹¹C-labeled tracers for PET imaging of $A\beta$ plaques in AD, we have evaluated a series of simple molecular probes. The minimum requirements for a

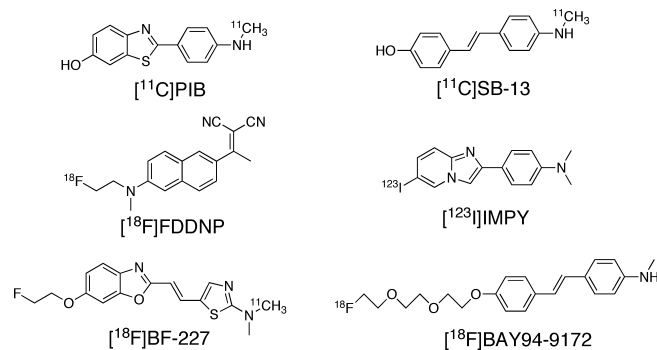
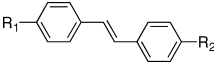


Fig. 1. Chemical Structure of $A\beta$ Imaging Probes Clinically Tested

Table 1. Inhibition Constants of Stilbene Derivatives on [¹²⁵I]TZDM Binding to Aβ(1–40) Aggregates


Compound	R ₁	R ₂	K _i (nM) ^{a)}
1	NO ₂	OCH ₃	151 ± 30
2	NH ₂	OCH ₃	36 ± 5
3	NHCH ₃	OCH ₃	1.2 ± 0.5
4	NHCH ₃	OH	6.0 ± 1.5
5	N(CH ₃) ₂	OCH ₃	1.3 ± 0.4
6	N(CH ₃) ₂	OH	2.2 ± 0.6

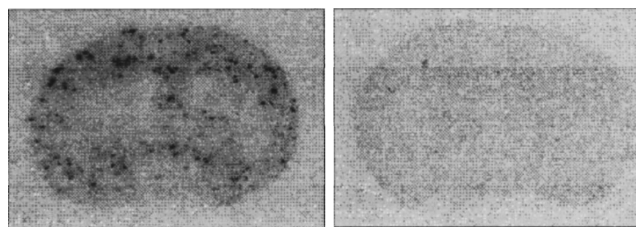
a) Values are means ± S.E. of three independent experiments.

successful Aβ-plaque-specific imaging agent include: small, neutral molecules; sufficient but moderate lipophilicity, good brain penetration; and low nonspecific binding in regions of the brain with no Aβ plaques. To meet the challenges of designing such molecules, we have investigated several series of core structures. One of them is a stilbene derivative, which is relatively simple and readily amenable to structural modification. A previous report suggested that the binding affinity to Aβ aggregates is associated with the essential substitution groups at the 4- and 4'-positions of the two phenol rings on the stilbene.²²⁾ To balance the need to preserve the binding affinity and provide compounds with moderate lipophilicity, we have studied a series of simple stilbenes with 4-amino and 4'-hydroxy substitution groups (Table 1).

An *in vitro* binding assay using preformed Aβ(1–40) aggregates demonstrated that substituted stilbenes (1–6) competed with [¹²⁵I]TZDM, binding to Aβ(1–40) aggregates with excellent binding affinities. Among the stilbenes evaluated, it is evident that *N*-mono-methylated (3, 4) or *N,N*-dimethylated (5, 6) derivatives displayed higher binding affinities (K_i = 1–6 nM). We are interested in selecting a compound with moderate lipophilicity and high binding affinity. To fulfill the need for opposing molecular properties, compound 4 (K_i = 6 nM) was selected as a compromise choice for ¹¹C labeling and further testing (Table 1).

In vitro autoradiography was performed by incubating [¹¹C]4 with brain sections from control and double-mutation mice (TgCRND8).^{23,24)} Using brain sections from these mice, Aβ plaque labeling by [¹¹C]4 was tested. The labeled stilbene derivative, [¹¹C]4, showed an excellent binding to plaques in the mutant mouse brain sections, while only minimal labeling in control sections was observed (Fig. 2).

To examine the *in vivo* brain penetration, normal rats were injected with [¹¹C]4, and cortex and cerebellar regional brain tissue uptakes were determined at different time points

Fig. 2. *In Vitro* Autoradiographic Detection of Aβ Plaques with [¹¹C]4 in TgCRND8 Mouse Brain Sections

Clear differences between histochemically characterized Tg Aβ(+) (left panel) and Tg Aβ(-) (right panel) brains are readily observable.

Table 2. Biodistribution of [¹¹C]4 in Normal Rats after Intravenous Injection (% ID/g)^{a)}

Time (min)	Cortex	Cerebellum	Blood
2	1.15 ± 0.08	1.15 ± 0.08	0.61 ± 0.07
15	0.74 ± 0.05	0.71 ± 0.01	0.39 ± 0.01
30	0.42 ± 0.03	0.41 ± 0.02	0.29 ± 0.01
60	0.30 ± 0.03	0.31 ± 0.01	0.24 ± 0.02

a) Expressed as % injected dose per gram. Each value represents the mean ± S.D. for 3 animals at each interval.

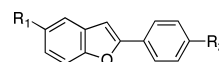


Fig. 3. Chemical Structure of Benzofuran Derivatives

Compounds here include the following: R₁ = OCH₃, OH; R₂ = NH₂, NHCH₃, N(CH₃)₂.

(Table 2). The initial brain uptake in the rat cortex was relatively high (1.15% dose/g, 2 min after intravenous (i.v.) injection), whereas the retention of [¹¹C]4 in the brain was low (0.3% dose/g, 60 min after i.v. injection). A rapid washout rate suggests that the compound has low nonspecific binding in the brain, a highly desirable property for an Aβ imaging probe. Taken together, the data strongly suggest that the new ¹¹C-labeled stilbene compound, [¹¹C]4, may be a useful PET tracer for imaging Aβ plaques in the brain of patients with AD.⁹⁾

In an attempt to develop more useful Aβ-specific imaging agents, we investigated a novel series of benzofuran derivatives, designed to be isosteric analogues of thioflavin-T (ThT) (Fig. 3).²⁵⁾ We reported previously that iodinated benzofuran derivatives displayed excellent binding affinities for Aβ(1–40) aggregates (K_i = 0.4–9.0 nM) and good brain penetration (>1.1% injected dose (ID) after i.v. injection in normal mice). However, the *in vivo* nonspecific binding of these probes, as reflected by their slow washout from the normal mouse brain, made them unsuitable for *in vivo* Aβ

Masahiro Ono is currently Associate Professor of Kyoto University. He was born in 1972 and graduated from Kyoto University in 1995. He received his Ph.D. in 2001 from Kyoto University under the supervision of Professor Hideo Saji. After that, he joined Nagasaki University under the supervision of Professor Morio Nakayama as an Assistant Professor in 2001. He worked as a postdoctoral fellow with Professor Hank F. Kung at the University of Pennsylvania for one and one-half years from 2001. He returned to Kyoto University and was promoted to Associate Professor in 2007. He received the Japanese Society of Nuclear Medicine Award for Young Scientists in 2008 and the Pharmaceutical Society of Japan Award for Young Scientists in 2009. His research interests are in the areas of radiopharmaceutical chemistry and molecular imaging.



Masahiro Ono

plaque imaging.²⁶⁾ These previous findings suggested that additional structural changes to these benzofurans may lead to the development of useful amyloid-specific imaging agents. Then, we designed and synthesized a new series of benzofuran derivatives (**7**–**12**) with low lipophilicity. An *in vitro* binding assay using AD brain homogenates demonstrated that substituted benzofuran derivatives competed with [¹²⁵I]IMPY binding to A β plaques with excellent binding affinities (Table 3). Comparing compounds **7**, **9**, and **11** with compounds **8**, **10**, and **12**, substitutions of the methoxy group at the 5-position with the hydroxy group resulted in only small changes in binding affinity. Compounds **9** and **10** with a monomethylaminophenyl moiety on the phenylbenzofuran molecule displayed slightly lower lipophilicity (higher binding affinity) as compared with compounds **7** and **8** with the aminophenyl moiety or compounds **11** and **12** with the dimethylaminophenyl moiety. However, all of the benzofuran derivatives evaluated maintained good binding affinity in the nanomolar range of K_i values. The results of the binding study strongly support our previous report that benzofuran derivatives have considerable tolerance for structural modification.²⁶⁾ Some reports showed that preserving the binding affinity for A β plaques and providing compounds with moderate lipophilicity are prerequisites for successful A β imaging agents. Thus we selected compound **10**, with moderate lipophilicity and the highest binding affinity for A β plaques in AD brain homogenates, for ¹¹C-labeling and additional studies.

Next, compound **10** was investigated for its neuropathologic staining of SPs in human AD brain sections (Fig. 4). Compound **10** stained neuritic plaques, as well as cerebrovascular amyloid (Fig. 4, panels A and B). Since it is commonly assumed that neuritic plaques are formed even in very mild AD cases, and that the density of the neuritic plaques is associated with the severity of dementia and the number of neurons,^{27,28)} clear staining of A β plaques with compound **10** demonstrates that it is a promising compound and deserves

further investigation as a potential tool for early diagnosis. Furthermore, compound **10** also displayed high binding affinity for NFTs in AD brain sections (Fig. 4C). A previous study reported that a marked increase in the amount of NFT accumulation in the hippocampus and entorhinal cortex was observed in the preclinical AD stage.²⁹⁾ Because compound **10** intensely stained NFTs in human AD brain sections, it could detect increased NFT accumulation in the hippocampus and entorhinal cortex of the AD brain. These findings from the neuropathologic staining of human AD brain sections suggest that compound **10** can bind to A β plaques and NFTs with almost the same pattern of FDDNP¹⁴⁾ or X-34³⁰⁾ previously reported, and quantitative evaluation of radiolabeled compound **10** in the brain may provide useful information on A β and tau pathology.

To predict the permeability of the blood–brain barrier (BBB), a 1-octanol/phosphate buffer (pH 7.4) partition coefficient of [¹¹C]**10** was examined. The log P value of [¹¹C]**10** was 2.36 at pH 7.4. Previous studies suggested that the optimal lipophilicity range for brain entry is observed for compounds with log P values between 1 and 3.³¹⁾ Below that range, passive diffusion through the BBB is poor; above that range, binding of any radiotracers to blood components (*e.g.*, red blood cells and albumin) is so great as to limit the amount available for brain entry. Since this ligand displayed moderate lipophilicity for BBB penetration, it was expected to show adequate brain uptake to detect A β plaques following systemic injection.

A biodistribution study in normal mice after intravenous injection showed that [¹¹C]**10** exhibited excellent brain uptake (4.8% ID/g of the brain at 2 min) and rapid washout (0.4 and 0.2% ID/g of the brain at 30 and 60 min, respectively), while the blood levels were relatively low at all time points measured (Table 4).

[¹¹C]PIB is currently the most widely utilized for detecting A β plaques in AD patients.^{6,32,33)} More recently, it has been reported that [¹¹C]**4** ([¹¹C]JSB-13) also showed performance

Table 3. Inhibition Constants of Benzofuran Derivatives Using [¹²⁵I]IMPY as the Ligand in AD Brain Gray Matter Homogenates

Compound	K_i (nM) ^{a)}
7	2.3±0.1
8	11.5±2.5
9	1.3±0.2
10	0.7±0.2
11	12.0±2.0
12	2.8±0.5

a) Values are means±S.E. of three independent experiments.

Table 4. Biodistribution of Radioactivity after Intravenous Injection of [¹¹C]**10** in Mice^{a)}

Time (min)	Brain	Blood
2	4.78 (1.10)	3.86 (0.36)
5	2.80 (0.63)	4.04 (1.14)
15	0.80 (0.31)	2.49 (0.67)
30	0.35 (0.08)	1.32 (0.41)
60	0.19 (0.04)	1.17 (0.14)

a) Expressed as % injected dose per gram. Each value represents the mean±S.D. for 4 animals at each interval.

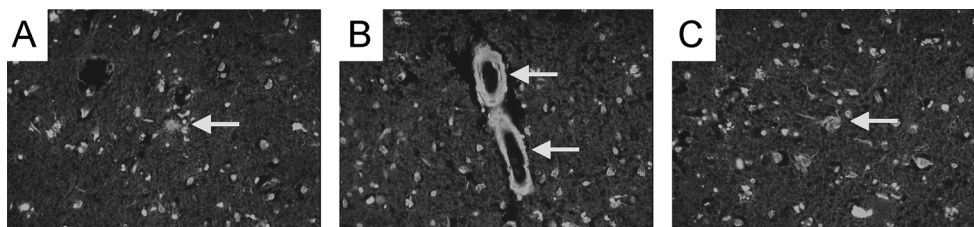


Fig. 4. Neuropathological Staining of Compound **10** on 5 μ m AD Brain Sections from the Temporal Cortex

(A) A β plaques are clearly stained with compound **10** ($\times 40$ magnification). (B) Many cerebrovascular amyloids are intensely stained with compound **10** ($\times 40$ magnification). (C) Compound **10** also stained neurofibrillary tangles (NFTs) ($\times 40$ magnification).

similar to that of the more established tracer, [^{11}C]PIB.¹⁰ Both tracers display appropriate properties for $A\beta$ imaging agents: high binding affinity for $A\beta$ plaques with K_i values of 4.3 and 6.0 nM for PIB and SB-13, respectively, in the *in vitro* binding assay; and high brain uptake and rapid clearance from the normal brain in animal studies. [^{11}C]PIB entered the brain rapidly (7.0% ID/g at 2 min after i.v. injection in mice) and cleared rapidly from normal mice brains (0.6% ID/g at 30 min after i.v. injection in mice). Since the ratio of 2–30-min mouse brain uptake after intravenous injection of [^{11}C]10 was 0.07, which is comparable to that of [^{11}C]PIB, [^{11}C]10 is also expected to have suitable *in vivo* pharmacokinetic properties for $A\beta$ imaging in AD patients, similar to [^{11}C]PIB.

To confirm the *in vivo* labeling of $A\beta$ plaques in the living mouse brain, we evaluated [^{11}C]10 using a model mouse of AD, Tg2576 mice, which are specifically engineered to over-produce $A\beta$ plaques in the brain. Autoradiographic images of Tg2576 mouse brain at 30 min after injection of [^{11}C]10 showed high radioactivity accumulation in the cerebral cortex and hippocampus (Fig. 5A). In contrast, wild-type mouse brain displayed no marked accumulation of [^{11}C]10 in the brain (Fig. 5A). Furthermore, we confirmed that the hot spots of [^{11}C]10 in Tg2576 brains corresponded with those of *in vitro* thioflavin-S (ThS) staining in the same brain section (Fig. 5, panels B and C). The specific *in vivo* labeling of $A\beta$ plaques demonstrates the feasibility of using it as an *in vivo* PET imaging agent for detecting $A\beta$ plaques in the brains of AD patients.

SPECT Probes for Imaging of $A\beta$ Plaques Derived from Flavonoid Compounds

Flavone-Based $A\beta$ Imaging Probes It is well known that PET provides better functional information with higher resolution and greater sensitivity than SPECT. However, since SPECT imaging is more practical as a routine clinical diagnostic procedure, the development of $A\beta$ imaging agents for SPECT has been highly anticipated. In an attempt to develop ^{123}I tracers for SPECT imaging, many radioiodinated probes based on various core structures have been studied. Among the radioiodinated ligands, [^{123}I]IMPY (Fig. 1) has been characterized as a potential SPECT imaging agent for $A\beta$ plaques.^{18,19} IMPY displayed selective $A\beta$ plaque labeling in *ex vivo* autoradiography using double-transgenic mice (PSAPP) as a model of AD.²⁰ In addition, 2-(3'-iodo-4'-aminophenyl)-6-hydroxybenzothiazole (6-OH-BTA-O-3'-I) also showed desirable *in vitro* and *in vivo* properties.³⁴ However, clinically useful SPECT imaging agents have not been reported in humans.

Recently, the effects of polyhydroxyflavones on the formation, extension, and destabilization of $A\beta$ aggregates have been studied *in vitro*.³⁵ These flavones dose dependently inhibited the formation of $A\beta$ aggregates, as well as destabilizing preformed $A\beta$ aggregates, indicating that they could interact directly with $A\beta$ aggregates. The findings in that previous report prompted us to apply flavones as a novel core structure of $A\beta$ imaging agents. Furthermore, some recent studies have shown that electron-donating groups such as methylamino, dimethylamino, methoxy, and hydroxy groups play a critical role in the binding affinity to $A\beta$ aggregates.^{5,9,19,22,26,36} With these considerations in mind, we de-

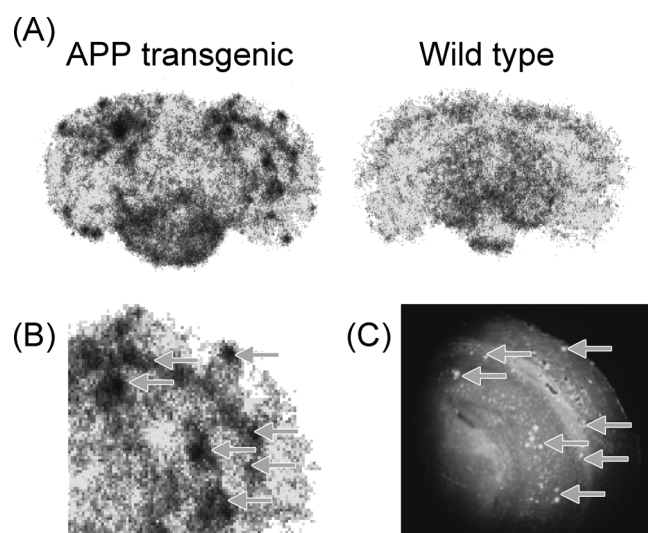


Fig. 5. *Ex Vivo* Plaque Labeling in Brain Sections from an APP Transgenic Mouse (A, B) and a Wild Type Mouse with [^{11}C]10 (A)

Amyloid plaques were confirmed by *in vitro* staining of the same section with thioflavin-S (C). Arrows show amyloid plaques labeled by both [^{11}C]10 and thioflavin-S.

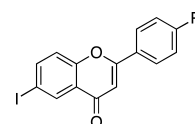


Fig. 6. Chemical Structure of Radioiodinated Flavone Derivatives

Compounds reported here include the following: R = NHMe (13), NMe₂ (14), OMe (15), OH (16).

signed four radioiodinated flavones with a radioiodine at the 6-position and an electron-donating group at the 4'-position (Fig. 6). Then we synthesized a series of flavone derivatives and evaluated their usefulness as *in vivo* SPECT $A\beta$ imaging agents.³⁷

Binding studies of [^{125}I]14 to aggregates of $A\beta(1-40)$ and $A\beta(1-42)$ were carried out. Transformation of the saturation binding of [^{125}I]14 to Scatchard plots gave linear plots, suggesting one binding site. [^{125}I]14 showed excellent binding affinity for both $A\beta(1-40)$ ($K_d = 12.4 \pm 2.3$ nM) and $A\beta(1-42)$ ($K_d = 17.4 \pm 5.7$ nM) aggregates (Fig. 7). Binding affinities of nonradioactive flavone derivatives (compounds 13, 14, 15, 16) were evaluated in inhibition studies against [^{125}I]14 binding on $A\beta(1-40)$ and $A\beta(1-42)$ aggregates. As shown in Table 5, all flavone derivatives competed well with [^{125}I]14 binding on $A\beta(1-40)$ and $A\beta(1-42)$ aggregates. The K_i values estimated for 13, 14, 15, and 16 were 23, 13, 29, and 73 nM for $A\beta(1-40)$ aggregates and 30, 16, 38, and 77 nM for $A\beta(1-42)$ aggregates, respectively. These K_i values suggest that the new series of flavones have high binding affinity for $A\beta(1-40)$ and $A\beta(1-42)$ aggregates in the following order: 14 > 13 > 15 > 16. No marked difference between $A\beta(1-40)$ and $A\beta(1-42)$ aggregates was observed in the K_i values. It is especially noteworthy that compounds 13, 14, 15, and 16 bound not only $A\beta(1-40)$ aggregates but also $A\beta(1-42)$ aggregates, as we aim to develop novel probes that can detect diffuse plaque deposits mainly composed of $A\beta(1-42)$. More interestingly, when ThT and Congo Red (CR) were evaluated for their competition against [^{125}I]14 binding on $A\beta(1-40)$ and $A\beta(1-42)$ aggregates,

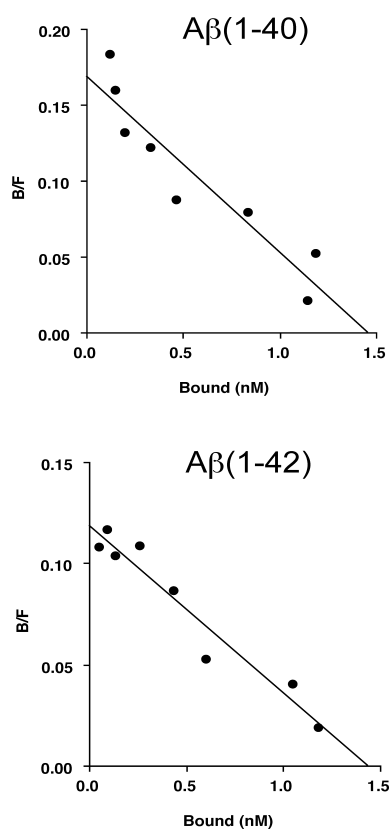


Fig. 7. Scatchard Plots of [¹²⁵I]14 Binding to Aggregates of Aβ(1—40) and Aβ(1—42)

[¹²⁵I]14 displayed one-site binding. High-affinity binding with K_d values in a nanomolar range was obtained ($K_d=12.3$ and 17.6 nM for Aβ(1—40) and Aβ(1—42) aggregates, respectively).

high K_i values (>1000 nM) were observed (Table 5), indicating poor binding competition. This finding suggests that these flavones may have a binding site on Aβ aggregates different from that of ThT and CR, although additional studies regarding the selectivity of binding affinity for Aβ aggregates are required.

Since the *in vitro* binding assays demonstrated the high binding affinity of the flavone derivatives for Aβ(1—40) and Aβ(1—42) aggregates, compounds **13**, **14**, **15**, and **16** were investigated for their neuropathologic staining of Aβ plaques and NFTs in human AD brain sections (Fig. 8). Compounds **13**, **14**, **15**, and **16** intensely stained Aβ plaques (Figs. 8A, E, I, M), neuritic plaques (Figs. 8B, F, J, N), and cerebrovascular amyloids (Figs. 8C, G, K, O) with nearly the same staining pattern. However, as seen in Figs. 8A, E, I, and M, these flavone compounds did not intensely stain the core region in so-called classic amyloid plaques, unlike the ThT and CR derivatives previously reported as Aβ imaging probes, indicating that flavone derivatives may have somewhat distinct binding characteristics for amyloid fibrils. The binding characteristics of the flavone derivatives for Aβ plaques in human AD

Table 5. Inhibition Constants (K_i , nM) of Compounds on Ligand Binding to Aggregates of Aβ(1—40) and Aβ(1—42)

Compound	Aβ(1—40)	Aβ(1—42)
13	22.6 ± 3.4	30.0 ± 3.4
14	13.2 ± 0.2	15.6 ± 2.4
15	29.0 ± 3.2	38.3 ± 8.1
16	72.5 ± 8.2	77.2 ± 9.2
ThT	>1000	>1000
CR	>1000	>1000

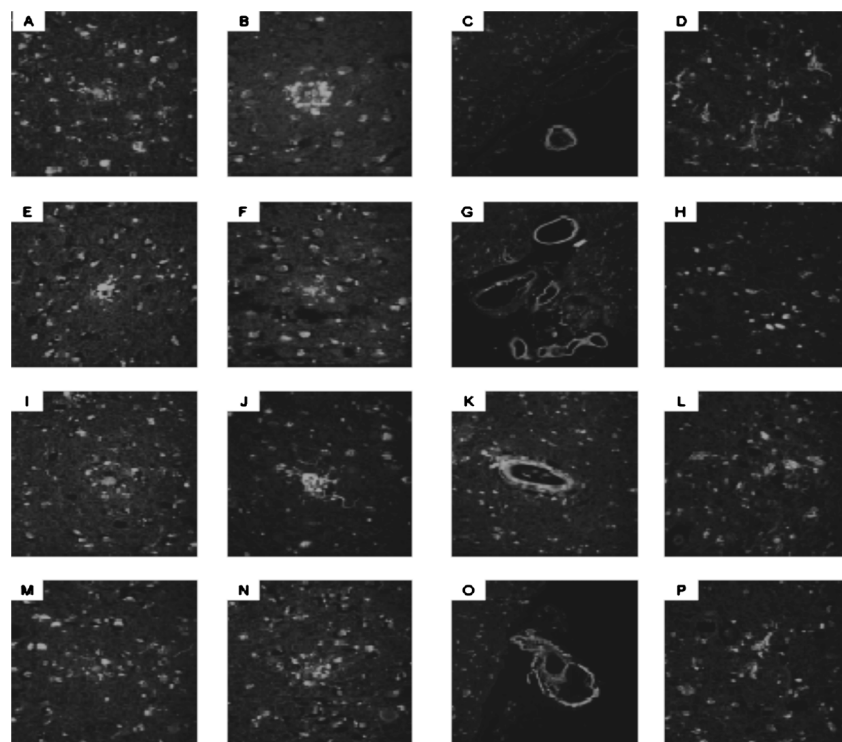


Fig. 8. Neuropathological Staining of Compounds **13** (A, E, I, M), **14** (B, F, J, N), **15** (C, G, K, O) and **16** (D, H, L, P) on $5 \mu\text{m}$ AD Brain Sections from the Temporal Cortex

(A) Aβ plaques (A—D) are clearly stained with compounds **13**, **14**, **15** and **16** ($\times 40$ magnification). Clear staining of neuritic plaques (E—H) and cerebrovascular amyloid (I—L) was also obtained. Many NFTs (M—P) are intensely stained with compounds **13**, **14**, **15** and **16** ($\times 40$ magnification).

sections may be relevant to the phenomenon observed in the *in vitro* binding assay: they may occupy a binding site on A β aggregates different from that of ThT and CR. Such a binding characteristic of the present flavone derivatives is thought to be related to the recent finding that a similar compound with a flavone backbone structure has binding affinity with amyloid fibrils and the APP sequence.³⁸⁾ However, this issue regarding the binding property of flavone derivatives remains unresolved. These flavone derivatives appear to stain not only neuritic amyloid plaque but also diffuse amyloid plaque deposits, which are known to be mainly composed of A β (1–42)³⁹⁾ and to be the initial pathologic change in AD.⁴⁰⁾ Thus flavone derivatives with high binding affinity for A β (1–42)-positive diffuse plaques may be more useful for presymptomatic detection of AD pathology. Furthermore, compounds **13**, **14**, **15**, and **16** also showed high binding affinity for NFTs in AD brain sections (Figs. 8D, H, L, P). These findings suggest that the flavone derivatives **13**, **14**, **15**, and **16** can bind amyloid fibrils and NFTs without the backbone structure of ThT or CR and that quantitative evaluation of their cerebral localization may provide useful information on A β and tau pathology.

Four radioiodinated flavone ligands ([¹²⁵I]**13**, [¹²⁵I]**14**, [¹²⁵I]**15**, and [¹²⁵I]**16**) were evaluated for their *in vivo* biodistribution in normal mice. All four ligands examined in this study displayed optimal lipophilicity as reflected by their logP values of 1.94, 2.69, 2.41, and 1.92 for [¹²⁵I]**13**, [¹²⁵I]**14**, [¹²⁵I]**15**, and [¹²⁵I]**16**, respectively. As expected, these ligands displayed high brain uptakes ranging from 3.2 to 4.1% ID/g brain at 2 min postinjection, indicating a level sufficient for brain imaging probes (Table 6). In addition, they displayed good clearance from the normal brain with 1.2, 1.0, 0.17, and 0.08% ID/g at 60 min postinjection for [¹²⁵I]**13**, [¹²⁵I]**14**, [¹²⁵I]**15**, and [¹²⁵I]**16**, respectively (Table 6). These values were equal to 29%, 27%, 4.3%, and 2.4% of the initial brain uptake peak for [¹²⁵I]**13**, [¹²⁵I]**14**, [¹²⁵I]**15**, and [¹²⁵I]**16**, respectively. Radioiodinated amyloid imaging agents such as [¹²⁵I]TZDM,³⁶⁾ [¹²⁵I]IBOX,⁴¹⁾ [¹²⁵I]*m*-1-stilbene,²²⁾ and [¹²⁵I]benzofuran²⁶⁾ reported previously showed high brain uptakes, but the washout rates from the normal brain were relatively slow. The slow washout rate from the brain leads to high background activity and prevents the visualization of A β plaques in the AD brain. The appropriate *in vivo* properties observed for radioiodinated flavones in the present study (higher brain uptake and faster washout from the normal brain) make them useful candidates for SPECT tracers for A β imaging.

Chalcone-Based A β Imaging Probes To search for more useful candidates in the development of *in vivo* A β imaging probes, we have designed a chemical modification of the flavone structure and selected the chalcone structure as a novel core for A β imaging probes (Fig. 9).^{42,43)} Chalcone is categorized as a member of the flavonoids containing flavone and has a chemical structure in which the ether linkage is removed from the flavone structure. Chalcone also contains a moiety structurally similar to curcumin (Fig. 9), which has been reported to have good brain permeability and favorable binding affinity to A β plaques after intravenous administration in Tg2576 transgenic mice.^{44,45)} Recently, radiolabeled curcumin derivatives have also been reported as A β imaging probes.⁴⁶⁾ In addition to the structural characteristics of chal-

Table 6. Biodistribution of Radioactivity after Intravenous Injection of [¹²⁵I]**13**, [¹²⁵I]**14**, [¹²⁵I]**15**, and [¹²⁵I]**16** in Mice^{a)}

Tissue	Time after injection (min)			
	2	10	30	60
[¹²⁵ I] 13				
Blood	1.89 (0.28)	1.39 (0.10)	1.34 (0.07)	1.50 (0.09)
Liver	16.28 (0.90)	25.28 (0.31)	18.61 (1.81)	15.14 (0.89)
Kidney	8.13 (1.28)	5.21 (0.44)	3.85 (0.33)	3.05 (0.25)
Intestine	3.10 (0.61)	7.91 (1.05)	12.84 (1.18)	21.48 (3.17)
Spleen	2.57 (1.54)	2.31 (0.01)	1.76 (0.23)	1.52 (0.29)
Heart	4.87 (0.66)	2.66 (0.12)	1.67 (0.14)	1.28 (0.12)
Stomach ^{b)}	0.78 (0.02)	0.87 (0.22)	1.44 (0.69)	1.80 (0.84)
Brain	4.12 (0.15)	3.68 (0.18)	1.84 (0.12)	1.19 (0.04)
[¹²⁵ I] 14				
Blood	1.87 (0.18)	1.07 (0.08)	1.20 (0.15)	1.15 (0.16)
Liver	15.41 (0.98)	21.85 (2.14)	15.71 (0.96)	12.40 (2.38)
Kidney	8.33 (1.47)	4.31 (0.28)	3.40 (0.31)	2.32 (0.45)
Intestine	2.24 (0.24)	6.56 (0.83)	12.97 (1.15)	18.64 (2.05)
Spleen	2.72 (0.20)	1.92 (0.33)	1.58 (0.31)	1.18 (0.17)
Heart	5.63 (0.80)	2.47 (0.14)	1.69 (0.06)	1.07 (0.17)
Stomach ^{b)}	0.73 (0.17)	0.63 (0.16)	1.17 (0.40)	1.06 (0.27)
Brain	3.22 (0.15)	3.61 (0.60)	1.89 (0.21)	0.99 (0.10)
[¹²⁵ I] 15				
Blood	1.87 (0.21)	1.19 (0.17)	0.40 (0.01)	0.23 (0.09)
Liver	8.96 (1.48)	9.01 (0.97)	3.75 (0.47)	1.88 (0.61)
Kidney	7.99 (1.08)	6.30 (1.02)	4.51 (1.59)	1.46 (1.12)
Intestine	3.52 (0.29)	14.39 (0.80)	22.51 (1.11)	30.05 (3.61)
Spleen	2.70 (0.08)	1.38 (0.37)	0.55 (0.30)	3.67 (5.89)
Heart	4.98 (0.41)	2.25 (0.40)	0.84 (0.14)	0.47 (0.22)
Stomach ^{b)}	0.68 (0.06)	0.45 (0.18)	0.55 (0.33)	0.31 (0.07)
Brain	4.00 (0.18)	2.36 (0.33)	0.51 (0.07)	0.17 (0.05)
[¹²⁵ I] 16				
Blood	2.77 (0.43)	1.58 (0.18)	0.66 (0.03)	0.20 (0.02)
Liver	9.77 (1.89)	8.24 (0.50)	6.80 (0.86)	4.78 (1.09)
Kidney	14.79 (2.59)	15.11 (2.00)	6.45 (0.84)	1.66 (0.62)
Intestine	3.12 (0.37)	11.26 (0.63)	22.01 (1.34)	27.28 (0.48)
Spleen	3.92 (1.18)	1.55 (0.15)	0.56 (0.13)	0.17 (0.06)
Heart	5.51 (0.71)	1.60 (0.18)	0.53 (0.04)	0.12 (0.02)
Stomach ^{b)}	0.89 (0.09)	0.59 (0.16)	1.56 (0.50)	0.81 (0.36)
Brain	3.31 (0.32)	1.90 (0.07)	0.52 (0.03)	0.08 (0.02)

a) Expressed as % injected dose per gram. Each value represents the mean \pm S.D. for 3–5 animals at each interval. b) Expressed as % injected dose per organ.

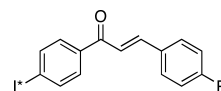
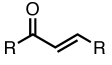


Fig. 9. Chemical Structure of Radioiodinated Chalcones

cone as the pharmacophore, some recent studies have shown that electron-donating groups such as amino, methylamino, dimethylamino, methoxy, or hydroxy groups play a critical role in the binding affinity to A β aggregates.^{9,22,26,36)} We therefore designed and synthesized novel chalcone derivatives and related chalcone-like compounds (**17–39**) (Fig. 10), and evaluated the effect of their structure–activity relationships on the binding affinity to A β aggregates and *in vivo* biodistribution using a compound with high binding affinity.

(E)-4-Dimethylamino-4'-[¹²⁵I]iodo-chalcone ([¹²⁵I]DMIC) was synthesized and used as the radioligand for competitive binding experiments (the K_d value of [¹²⁵I]DMIC is 4.2 nM).⁴²⁾ Binding affinities of chalcone and chalcone-like compounds were evaluated in inhibition assays against [¹²⁵I]DMIC binding on A β (1–42) aggregates (Table 7). The K_i values suggested that the new series of chalcone and chal-

Table 7. Inhibition Constants of Chalcone and Chalcone-Like Derivatives on Ligand Binding to A β (1–42) Aggregates

Compd.			K_i (nM) ^(d)
	R	R'	
17	4-Aminophenyl	4-Iodophenyl	248 ± 56
18	4-Methylaminophenyl	4-Iodophenyl	23.9 ± 3.6
19	4-Dimethylaminophenyl	4-Iodophenyl	13.3 ± 1.9
20	5-Iodo-2-thienyl	4-Aminophenyl	121 ± 40
21	5-Iodo-2-thienyl	4-Methylaminophenyl	14.1 ± 0.6
22	5-Iodo-2-thienyl	4-Dimethylaminophenyl	3.9 ± 0.4
23	4-Aminophenyl	5-Bromo-2-thienyl	476 ± 48
24	4-Methylaminophenyl	5-Bromo-2-thienyl	198 ± 49
25	4-Dimethylaminophenyl	5-Bromo-2-thienyl	106 ± 7.1
26	4-Iodophenyl	Phenyl	151 ± 16
27	4-Iodophenyl	2-Furanyl	908 ± 212
28	4-Iodophenyl	3-Furanyl	125 ± 9.2
29	4-Iodophenyl	2-Thienyl	102 ± 16
30	4-Iodophenyl	3-Thienyl	93 ± 11
31	4-Iodophenyl	2-Imidazolyl	797 ± 316
32	4-Iodophenyl	2-Thiazoyl	>10000
33	4-Iodophenyl	5-Dimethylamino-2-furanyl	1132 ± 344
34	4-Iodophenyl	5-Dimethylamino-2-thienyl	113 ± 10
35	5-Iodo-2-thienyl	5-Dimethylamino-2-thienyl	137 ± 3.4
36	5-Iodo-2-thienyl	5-Dimethylamino-2-furanyl	1608 ± 85
37	5-Bromo-2-furanyl	4-Dimethylaminophenyl	126 ± 13
38	5-Bromo-2-furanyl	5-Dimethylamino-2-thienyl	2648 ± 222
39	5-Bromo-2-furanyl	5-Dimethylamino-2-furanyl	>10000
CR	—	—	>10000
ThT	—	—	>10000
AIC ^(b)	4-Iodophenyl	4-Aminophenyl	105 ± 12
IMC ^(c)	4-Iodophenyl	4-Methylaminophenyl	6.3 ± 1.6
DMIC ^(d)	4-Iodophenyl	4-Dimethylaminophenyl	2.9 ± 0.3

a) Values are means ± S.E. of 3–6 independent experiments. b) 4-Amino-4'-iodo-chalcone. c) 4'-Iodo-4-methylamino-chalcone. d) 4-Dimethylamino-4'-iodo-chalcone. b, c, d) Our unpublished data.⁴²⁾

cone-like compounds had high binding affinity for A β (1–42) aggregates in the order of *N,N*-dimethylated derivatives (19, 20) > *N*-monomethylated derivatives (18, 37) > primary amino derivatives (17, 35) when comparing similar core structures. Compounds 17, 18, and 19 with a substituted group at the 4'-position and iodine at the 4-position displayed higher K_i values (lower binding affinities) as compared with compounds 4-amino-4'-iodo-chalcone (AIC), 4'-iodo-4-methylamino-chalcone (IMC), and DMIC, which have a substituted group and iodine at the inverse position against compounds 17, 18, and 19. The K_i values of 36, 38, and 39 with a thienyl group at the R-position and phenyl group at the R'-position were higher than those of 35, 37, and 20 with a phenyl group at the R-position and thienyl group at the R'-position, indicating that the binding affinities depend on the combination of heterocycles introduced at the R- and R'-positions and not on the position of the substituted group or iodine (bromine) group. When comparing the K_i values of heterocyclic compounds with the same substituted group, the binding affinities increased in the order of phenyl > thienyl > furanyl at the R-position and phenyl = thienyl > furanyl at the R'-position. The K_i values of compounds without the substituted group on the ring at the R'-position (21–27) were varied by altering the type of heterocycle. Furthermore, to obtain information on the binding site of the new chalcone-like compounds, inhibition studies were carried out using CR and ThT, which are well-known proto-

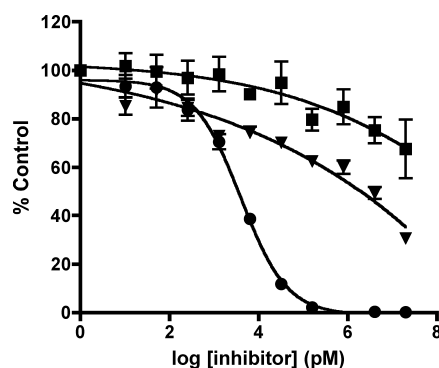
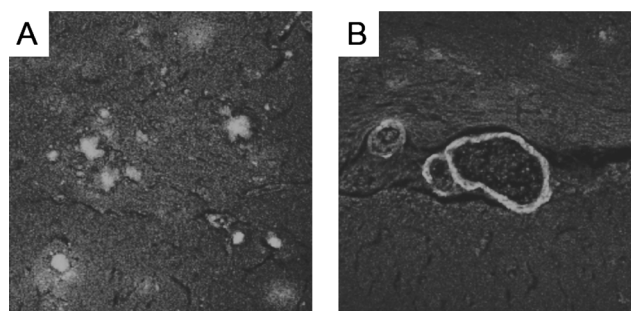
Fig. 10. Competition Curves of [¹²⁵I]DMIC against Compound 20 (Closed Circle), CR (Closed Square), and ThT (Closed Triangle)

Fig. 11. Neuropathological Fluorescent Staining of Compound 20 on AD Model Mouse Brain Sections

(A) Compound 20 intensely stained A β plaques. (B) Clear staining of cerebrovascular amyloids was also observed.

Table 8. Brain Uptake of Radioactivity after Intravenous Injection of [¹²⁵I]20 in Mice^(a)

	Time after injection (min)			
	2	10	30	60
	2.46 (0.30)	0.75 (0.31)	0.31 (0.04)	0.21 (0.02)

a) Expressed as % injected dose per gram. Each value represents the mean ± S.D. for five mice at each interval.

types of A β imaging probes. While compound 20 competed for [¹²⁵I]DMIC binding to A β (1–42) aggregates, CR and ThT did not exhibit a dose-dependent decrease in the specific binding of [¹²⁵I]DMIC (Fig. 10).

To confirm the binding affinity to A β plaques in the AD brain, fluorescent staining of AD model mouse brain sections was carried out using the fluorescence of compound 20 (Fig. 11). Compound 20 intensely stained A β plaques in the brain sections. Also, clear staining of cerebrovascular amyloid was observed. This result suggests that compound 20 should detect A β plaques in AD brains.

The radioiodinated compound [¹²⁵I]20 was evaluated for its *in vivo* biodistribution in normal mice (Table 8). Initial brain uptake of [¹²⁵I]20 was 2.46% of injected dose/g at 2 min after intravenous injection, whereas the radioactivity accumulated in the brain was rapidly eliminated (0.21% of injected dose/g, 60 min postinjection), indicating highly desirable properties for an A β imaging agent. Taken together, the data suggest that [¹²⁵I]20 should be further investigated as a potentially useful β -amyloid imaging probe.

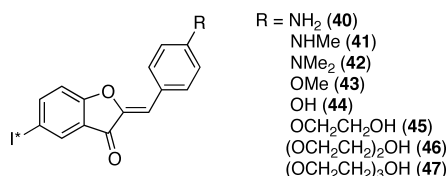
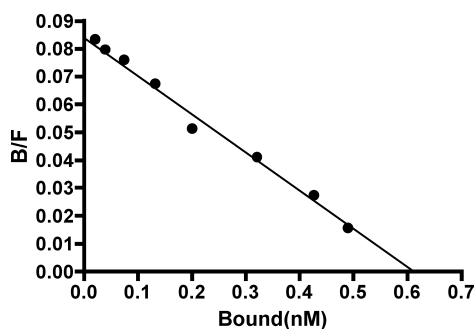


Fig. 12. Chemical Structure of Aurone Derivatives

Fig. 13. Scatchard Plots of [¹²⁵I]**40** Binding to Aβ(1—42) Aggregates
 High binding affinity with a K_d value in a nanomolar range was obtained.

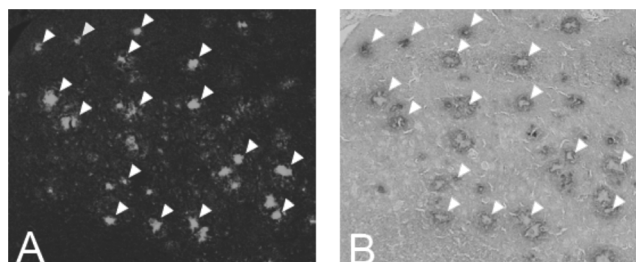
Aurone-Based Aβ Imaging Probes To explore more useful candidates for core structures of Aβ imaging probes, we selected one of the flavonoids, aurone, as a new core structure. First, we synthesized a series of aurone derivatives, which possess a radioiodine at the 5-position and a nucleophilic group (NH₂, NHMe, NMe₂) at the 4'-position, and evaluated their biological activities as *in vivo* Aβ imaging probes (Fig. 12).⁴⁷⁾ To evaluate the binding affinity of aurone derivatives to Aβ aggregates, a saturation assay with [¹²⁵I]**40** was carried out using Aβ(1—42) aggregates. When the saturation bindings of [¹²⁵I]**40** were transformed to Scatchard plots, they showed linear plots, indicating that aurone derivatives have one binding site on Aβ aggregates (Fig. 13). [¹²⁵I]**40** displayed excellent binding affinity for Aβ(1—42) aggregates with a K_d value of 7.9 ± 1.3 nM. Binding affinities of nonradioactive aurones (**40**, **41**, **42**) were also evaluated with inhibition studies against [¹²⁵I]**40** binding on Aβ(1—42) aggregates (Table 9). The K_i values estimated for **40**, **41**, and **42** were 2.7, 1.2, and 6.8 nM for Aβ(1—42) aggregates, respectively. These K_i values suggested that the new series of aurones had excellent binding affinity for Aβ(1—42) aggregates and showed considerable tolerance for structural modification. The K_i values of the radioiodinated aurones reported previously were lower than those of the radioiodinated flavones, indicating that the radioiodinated aurones have higher binding affinities to Aβ plaques than those of the corresponding radioiodinated flavones and chalcones.

To confirm the binding affinity of aurone derivatives to Aβ plaques in the brain, neuropathologic fluorescent staining with compound **42** was carried out using double-transgenic Alzheimer's mouse brain sections (Fig. 14). Many Aβ plaque deposits were clearly stained with compound **42**, as reflected by the high binding affinity to Aβ aggregates in *in vitro* competition assays. The compound clearly stained not only core plaques, but also typical senile plaques. The labeling pattern was consistent with that observed with immunohistochemical labeling with an antibody specific for Aβ, indicating that aurone derivatives show specific binding to Aβ plaques. Thus

Table 9. Inhibition Constants of Aurone Derivatives on Ligand Binding to Aβ(1—42) Aggregates

Compound	K_i (nM) ^{a)}
40	2.69 ± 0.16
41	1.24 ± 0.11
42	6.82 ± 0.48

a) Values are means \pm S.E. of three independent experiments.

Fig. 14. Neuropathological Staining of Compound **42** on 5 μm AD Model Mouse Sections from the Cortex

(A) Many Aβ plaques are clearly stained with compound **42**. (B) The same sections were immunostained using an antibody against Aβ.

Table 10. Biodistribution of Radioactivity after Intravenous Injection of [¹²⁵I]**40**, [¹²⁵I]**41**, and [¹²⁵I]**42** in Mice^{a)}

Compound	Time after injection (min)			
	2	10	30	60
[¹²⁵ I] 40	4.57 (0.27)	1.51 (0.17)	0.49 (0.06)	0.26 (0.03)
[¹²⁵ I] 41	3.17 (0.45)	1.22 (0.09)	0.32 (0.02)	0.24 (0.03)
[¹²⁵ I] 42	1.89 (0.38)	0.69 (0.21)	0.26 (0.04)	0.11 (0.03)

a) Expressed as % injected dose per gram. Each value represents the mean \pm S.D. for five mice at each interval.

the results suggest that aurone derivatives may be applicable for *in vivo* imaging of Aβ plaques in the brain.

To evaluate the brain uptake of the aurone derivatives, *in vivo* biodistribution studies in normal mice were performed with three radioiodinated aurones ([¹²⁵I]**40**, [¹²⁵I]**41**, and [¹²⁵I]**42**) (Table 10). The aurone derivatives displayed high brain uptake rates ranging from 1.9—4.6% ID/g brain at 2 min postinjection, indicating a level sufficient for Aβ imaging of the brain. In addition, they displayed rapid clearance from the normal brain with 0.49%, 0.32%, and 0.26% ID/g at 30 min postinjection for [¹²⁵I]**40**, [¹²⁵I]**41**, and [¹²⁵I]**42**, respectively. These values were equal to 10.7%, 10.1%, and 13.8% of the initial brain uptake peak for [¹²⁵I]**40**, [¹²⁵I]**41**, and [¹²⁵I]**42**, respectively. We reported that radioiodinated flavones showed high brain uptake (3.2—4.1% ID/g at 2 min postinjection) and good clearance from the brain (0.5—1.9% ID/g at 30 min postinjection). However, the ratios of 2- to 30-min mouse brain uptake of the radioiodinated flavones were 40.0%, 44.6%, and 57.8% for NH₂, NHMe, and NMe₂ derivatives, respectively, which were higher than those of radioiodinated aurones. The result suggests that aurone derivatives do not show high nonspecific binding in the brain *in vivo*. These desirable pharmacokinetics demonstrated by radioiod-

inated aurones are critical to detect A β plaques in the AD brain. These biodistribution data suggest that novel radioiodinated aurones may have more suitable *in vivo* pharmacokinetic properties for A β imaging in AD brains compared with the radioiodinated flavones and chalcones. However, these aurone derivatives appeared inferior to IMPY in pharmacokinetics, although their high affinity for A β plaques is sufficient for imaging *in vivo*. Therefore additional structural changes are essential to improve the properties of aurone derivatives to make them suitable for the imaging of A β plaques in the brain.

To develop more promising aurones for SPECT-based imaging of A β plaques, we designed a novel series of radioiodinated derivatives with polyethylene glycol (PEG).⁴⁸ PEG is nontoxic, nonimmunogenic, highly soluble in water, and FDA approved, and PEGylation has been used to change the pharmacokinetics of various biologically interesting proteins or peptides, leading to better therapeutics.^{49,50} Therefore PEGylated aurone derivatives are worthy of further evaluation as novel A β imaging probes for SPECT.

We designed and synthesized a novel series of radioiodinated aurone derivatives with not only 1 to 3 units of ethylene glycol at the 4' position, but also other nucleophilic groups ($-\text{OCH}_3$ and $-\text{OH}$) (Fig. 12) and evaluated their biological potential as probes for imaging A β by testing their affinity for A β aggregates *in vitro* and their uptake by and clearance from the brain in biodistribution experiments using normal mice.

Our initial screening of the affinity of aurone derivatives (**43**, **44**, **45**, **46**, **47**) was carried out with A β (1–42) aggregates, using [¹²⁵I]AAU as the competing radioligand (Table 11). The K_i values estimated for **43**, **44**, **45**, **46**, and **47** were 2.9, 1.3, 1.1, 3.4, and 2.6 nM, respectively. These values suggested that the new series of aurone derivatives had binding affinity for A β (1–42) aggregates despite their substituted groups. The binding affinity is in the same range as that of aurone derivatives possessing a nucleophilic group (NH_2 , NHMe , NMe_2).⁴⁷ These results clearly indicate that aurone derivatives exhibit considerable tolerance to structural modifications. The binding affinity of aurone derivatives is very close to that of known A β imaging probes such as SB-13 ($K_i=1.2$ nM,⁵¹) PIB ($K_i=2.8$ nM,⁵²) and IMPY ($K_i=1.4$ nM,⁵¹) indicating that they have sufficient affinity to test clinically.

To confirm the affinity of aurone derivatives for A β plaques in the mouse brain, neuropathologic fluorescent staining with **43**, **44**, **45**, **46**, and **47** was carried out using double-transgenic Alzheimer's mouse brain sections (Fig. 15). Many A β plaque deposits were clearly stained with the derivatives, as reflected by the high binding affinity for A β aggregates in *in vitro* competition assays. The labeling pattern was consistent with that observed with ThS. These results suggest that novel aurone derivatives show affinity for A β plaques in the mouse brain in addition to having binding affinity for synthetic A β 42 aggregates.

To evaluate brain uptake of the aurone derivatives, biodistribution experiments were performed in normal mice with five radioiodinated aurones ([¹²⁵I]**43**, [¹²⁵I]**44**, [¹²⁵I]**45**, [¹²⁵I]**46**, and [¹²⁵I]**47**) (Table 12). Radioactivity after injection of the aurone derivatives penetrated the BBB and showed excellent uptake ranging from 1.7 to 4.5% ID/g brain at 2 min

Table 11. Inhibition Constants of Newly Synthesized Aurone Derivatives for the Binding of Ligands to A β (1–42) Aggregates

Compound	K_i (nM) ^{a)}
43	2.89 \pm 0.42
44	1.28 \pm 0.29
45	1.05 \pm 0.06
46	3.36 \pm 0.29
47	2.56 \pm 0.31

a) Data are the mean \pm S.E. for two independent measurements done in triplicate.

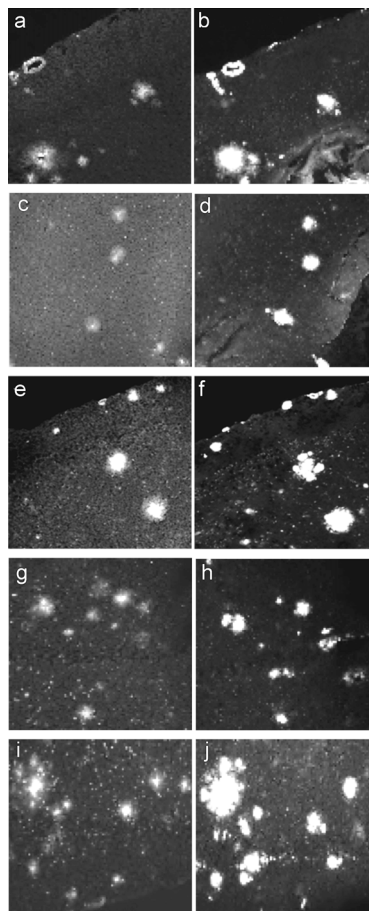


Fig. 15. Neuropathological Staining of **43**, **44**, **45**, **46**, and **47** (a, c, e, g, i) in 10 μm Sections from a Mouse Model of AD

Labeled plaques were confirmed by staining of the adjacent sections with ThS (b, d, f, h, j).

postinjection, a level sufficient for imaging A β plaques in the brain. In addition, it displayed good clearance from the normal brain with 0.1–0.4% ID/g at 30 min postinjection. One method to select a ligand with appropriate *in vivo* kinetics is to use $\text{brain}_{2\text{min}}/\text{brain}_{30\text{min}}$ as an index to compare the washout rate. The five radioiodinated aurone derivatives [¹²⁵I]**43**, [¹²⁵I]**44**, [¹²⁵I]**45**, [¹²⁵I]**46**, and [¹²⁵I]**47** showed $\text{brain}_{2\text{min}}/\text{brain}_{30\text{min}}$ ratios of 15.4, 8.3, 18.8, 9.7, and 15.6, respectively. [¹²⁵I]**45** had the best washout index. Previously reported radioiodinated aurones showed high uptake (1.9–4.6% ID/g at 2 min postinjection) and good clearance from the brain (0.3–0.5% ID/g at 30 min postinjection).⁴⁸ However, the $\text{brain}_{2\text{min}}/\text{brain}_{30\text{min}}$ ratios of these compounds were 7.3–9.9, lower than that of [¹²⁵I]**45**, indicating that [¹²⁵I]**45** could clear more rapidly from the normal mouse brain than

Table 12. Biodistribution of Radioactivity after Injection of Aurone Derivatives in Mice^{a)}

Tissue	Time after injection (min)			
	2	10	30	60
¹²⁵ I]43				
Blood	3.16 (0.82)	1.51 (0.23)	0.95 (0.19)	0.70 (0.60)
Liver	6.87 (2.18)	5.16 (0.73)	2.76 (0.40)	1.86 (0.83)
Kidney	7.26 (2.18)	7.00 (1.49)	4.93 (1.52)	2.43 (1.17)
Intestine	1.59 (0.51)	4.70 (1.46)	11.67 (3.56)	9.02 (3.14)
Spleen	1.45 (0.56)	0.74 (0.10)	0.48 (0.10)	0.43 (0.14)
Pancreas	2.83 (0.75)	0.77 (0.17)	0.62 (0.75)	0.16 (0.05)
Heart	3.84 (1.04)	1.06 (0.10)	0.37 (0.09)	0.25 (0.12)
Stomach ^{b)}	0.39 (0.20)	0.89 (0.48)	0.42 (0.13)	0.82 (0.46)
Brain	1.69 (0.43)	0.54 (0.12)	0.11 (0.05)	0.03 (0.02)
¹²⁵ I]44				
Blood	3.14 (0.39)	2.77 (0.28)	1.75 (0.38)	0.87 (0.28)
Liver	6.05 (1.49)	6.63 (1.08)	4.23 (0.63)	4.45 (3.14)
Kidney	11.08 (2.96)	11.22 (2.26)	5.82 (1.11)	2.43 (1.04)
Intestine	2.11 (0.75)	6.12 (0.83)	12.67 (2.13)	14.87 (5.42)
Spleen	2.18 (0.48)	1.36 (0.83)	0.69 (0.14)	0.42 (0.02)
Pancreas	5.28 (0.99)	2.65 (0.64)	0.92 (0.19)	0.36 (0.09)
Heart	6.23 (0.63)	2.57 (0.41)	0.98 (0.14)	0.42 (0.14)
Stomach ^{b)}	0.93 (0.28)	1.46 (0.23)	1.22 (0.72)	1.89 (1.01)
Brain	3.07 (0.39)	1.48 (0.19)	0.37 (0.07)	0.14 (0.12)
¹²⁵ I]45				
Blood	4.97 (0.96)	3.88 (1.09)	2.38 (0.85)	1.24 (0.35)
Liver	13.4 (3.20)	13.3 (2.59)	7.60 (1.95)	5.27 (0.64)
Kidney	11.3 (1.23)	10.8 (2.58)	6.09 (2.43)	2.50 (1.30)
Intestine	2.78 (0.42)	7.83 (2.22)	17.82 (3.58)	20.93 (4.46)
Spleen	2.72 (0.28)	1.02 (0.22)	0.50 (0.13)	0.21 (0.09)
Pancreas	6.38 (0.63)	1.61 (0.61)	0.59 (0.21)	0.29 (0.15)
Heart	6.30 (0.65)	2.30 (0.46)	0.83 (0.15)	0.72 (0.58)
Stomach ^{b)}	1.88 (0.41)	3.23 (2.58)	5.15 (4.43)	1.45 (0.78)
Brain	4.51 (0.25)	1.48 (0.28)	0.24 (0.03)	0.09 (0.04)
¹²⁵ I]46				
Blood	3.61 (0.74)	5.18 (2.54)	1.11 (0.73)	0.68 (0.45)
Liver	12.5 (3.21)	11.6 (1.75)	9.31 (2.66)	7.12 (4.05)
Kidney	12.0 (0.99)	10.3 (1.17)	5.75 (1.53)	2.55 (1.12)
Intestine	2.35 (1.33)	8.18 (2.32)	19.7 (7.86)	26.38 (5.95)
Spleen	2.26 (0.53)	1.56 (0.45)	0.78 (0.26)	0.45 (0.21)
Pancreas	5.67 (2.72)	2.24 (0.68)	1.40 (0.44)	0.39 (0.29)
Heart	6.04 (0.38)	2.77 (0.94)	1.21 (0.66)	0.66 (0.57)
Stomach ^{b)}	1.71 (0.38)	5.65 (6.63)	5.00 (2.83)	6.58 (4.59)
Brain	3.69 (0.22)	1.53 (0.31)	0.38 (0.05)	0.16 (0.03)
¹²⁵ I]47				
Blood	2.98 (0.64)	4.62 (2.17)	0.83 (0.64)	0.51 (0.31)
Liver	12.95 (3.43)	11.20 (1.51)	8.34 (1.98)	7.70 (3.93)
Kidney	11.58 (1.13)	9.66 (2.28)	5.84 (1.79)	2.41 (1.22)
Intestine	2.52 (0.39)	7.50 (4.85)	17.95 (7.53)	22.64 (5.89)
Spleen	2.26 (0.65)	1.40 (0.23)	0.84 (0.23)	0.56 (0.24)
Pancreas	5.51 (0.59)	1.84 (0.44)	0.87 (0.37)	0.79 (0.70)
Heart	5.67 (1.02)	2.24 (0.56)	1.40 (0.49)	0.39 (0.68)
Stomach ^{b)}	3.29 (1.47)	4.73 (5.14)	7.45 (4.62)	7.61 (5.20)
Brain	2.81 (0.19)	2.32 (0.21)	0.18 (0.06)	0.08 (0.04)

a) Each value represents the mean ± S.D. for 4–5 animals. b) Expressed as % injected dose per organ.

aurones with amino groups. It has been reported that [¹²⁵I]IMPY enters the brain rapidly (2.88% ID at 2 min postinjection) and was cleared from the normal brain (0.26% ID at 30 min postinjection), indicating the brain_{2min}/brain_{30min} ratio to be 11.1.¹⁹⁾ The aurone derivatives reported in this study appear superior to IMPY in pharmacokinetics, in addition to showing similar binding affinities sufficient for the imaging of A β plaques *in vivo*. The pharmacokinetics demonstrated by [¹²⁵I]45 are critical to the detection of A β plaques in the AD brain.

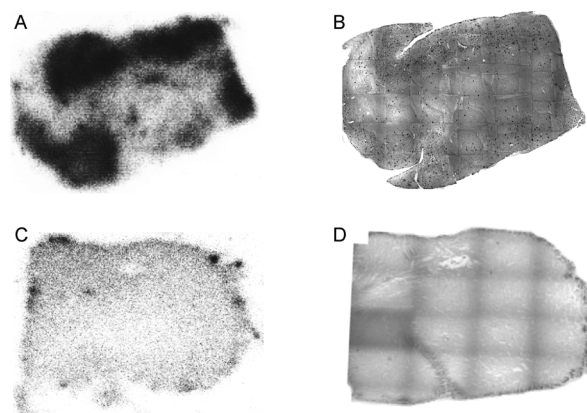


Fig. 16. *In Vitro* Autoradiography of [¹²⁵I]45 for Labeling of A β Plaques in AD Brain Sections

In vitro autoradiography of [¹²⁵I]45 reveals a distinct labeling of A β plaques in AD brain sections (A). Under similar conditions, there is very little labeling of [¹²⁵I]45 in control brain section (C). The presence and localization of A β plaques in the sections were confirmed with immunohistochemical staining using a monoclonal A β antibody (B, D).

Next, [¹²⁵I]45 was investigated for its binding affinity for A β plaques using *in vitro* autoradiography in human AD brain sections (Fig. 16). Autoradiographic images of [¹²⁵I]45 showed high levels of radioactivity in the brain sections (Fig. 16A). Furthermore, we confirmed that the hot spots of [¹²⁵I]45 corresponded with those of *in vitro* immunohistochemical staining in the same brain sections (Fig. 16B). In contrast, normal human brain displayed no remarkable accumulation of [¹²⁵I]45 (Fig. 16C), correlating well with the absence of A β plaques (Fig. 16D). These results demonstrate the feasibility of using [¹²⁵I]45 as a probe for detecting A β plaques in the brains of AD patients with SPECT.

Conclusion

We successfully designed and synthesized several basic structures that can function as useful A β imaging probes. We hope that the A β imaging probes will contribute to improved diagnosis and accelerate the discovery of effective therapeutic agents for AD in the near future.

Acknowledgments All the results in this review were obtained at the University of Pennsylvania, Nagasaki University, and Kyoto University. I would like to express sincere appreciation to Professor Hank F. Kung, Professor Morio Nakayama, and Professor Hideo Saji for their helpful, continuous advice and support. The research reviewed in this paper was possible only through the dedication, enthusiasm, and creativity of all my coworkers, whose names are acknowledged in the publications from our laboratory cited here. These studies were supported by a Grant-in Aid for Young Scientists (A) and (B) from the Ministry of Education, Culture, Sports, Science and Technology, the Industrial Technology Research Grant Program from New Energy and Industrial Technology Development Organization (NEDO), the Program for Promotion of Fundamental Biomedical Innovation (NIBIO), and a Health Labour Sciences Research Grant.

References

- 1) Klunk W. E., *Neurobiol. Aging*, **19**, 145–147 (1998).
- 2) Selkoe D. J., *Physiol. Rev.*, **81**, 741–766 (2001).
- 3) Mathis C. A., Wang Y., Klunk W. E., *Curr. Pharm. Des.*, **10**, 1469–1492 (2004).
- 4) Nordberg A., *Lancet Neurol.*, **3**, 519–527 (2004).
- 5) Mathis C. A., Wang Y., Holt D. P., Huang G. F., Debnath M. L., Klunk W. E., *J. Med. Chem.*, **46**, 2740–2754 (2003).
- 6) Klunk W. E., Engler H., Nordberg A., Wang Y., Blomqvist G., Holt D. P., Bergstrom M., Savitcheva I., Huang G. F., Estrada S., Aussen B.,

- Debnath M. L., Barletta J., Price J. C., Sandell J., Lopresti B. J., Wall A., Koivisto P., Antoni G., Mathis C. A., Langstrom B., *Ann. Neurol.*, **55**, 306—319 (2004).
- 7) Klunk W. E., Mathis C. A., Price J. C., Lopresti B. J., DeKosky S. T., *Brain*, **129**, 2805—2807 (2006).
- 8) Rowe C. C., Ng S., Ackermann U., Gong S. J., Pike K., Savage G., Cowie T. F., Dickinson K. L., Maruff P., Darby D., Smith C., Woodward M., Merory J., Tochon-Danguy H., O'Keefe G., Klunk W. E., Mathis C. A., Price J. C., Masters C. L., Villemagne V. L., *Neurology*, **68**, 1718—1725 (2007).
- 9) Ono M., Wilson A., Nobrega J., Westaway D., Verhoeff P., Zhuang Z. P., Kung M. P., Kung H. F., *Nucl. Med. Biol.*, **30**, 565—571 (2003).
- 10) Verhoeff N. P., Wilson A. A., Takeshita S., Trop L., Hussey D., Singh K., Kung H. F., Kung M. P., Houle S., *Am. J. Geriatr. Psychiatry*, **12**, 584—595 (2004).
- 11) Rowe C. C., Ackerman U., Browne W., Mulligan R., Pike K. L., O'Keefe G., Tochon-Danguy H., Chan G., Berlangieri S. U., Jones G., Dickinson-Rowe K. L., Kung H. P., Zhang W., Kung M. P., Skovronsky D., Dyrks T., Holl G., Krause S., Friebe M., Lehman L., Lindemann S., Dinkelborg L. M., Masters C. L., Villemagne V. L., *Lancet Neurol.*, **7**, 129—135 (2008).
- 12) Zhang W., Oya S., Kung M. P., Hou C., Maier D. L., Kung H. F., *Nucl. Med. Biol.*, **32**, 799—809 (2005).
- 13) Kudo Y., Okamura N., Furumoto S., Tashiro M., Furukawa K., Maruyama M., Itoh M., Iwata R., Yanai K., Arai H., *J. Nucl. Med.*, **48**, 553—561 (2007).
- 14) Agdeppa E. D., Kepe V., Liu J., Flores-Torres S., Satyamurthy N., Petric A., Cole G. M., Small G. W., Huang S. C., Barrio J. R., *J. Neurosci.*, **21**, RC189 (2001).
- 15) Shoghi-Jadid K., Small G. W., Agdeppa E. D., Kepe V., Ercoli L. M., Siddarth P., Read S., Satyamurthy N., Petric A., Huang S. C., Barrio J. R., *Am. J. Geriatr. Psychiatry*, **10**, 24—35 (2002).
- 16) Small G. W., Kepe V., Ercoli L. M., Siddarth P., Bookheimer S. Y., Miller K. J., Lavretsky H., Burggren A. C., Cole G. M., Vinters H. V., Thompson P. M., Huang S. C., Satyamurthy N., Phelps M. E., Barrio J. R., *N. Engl. J. Med.*, **355**, 2652—2663 (2006).
- 17) Braskie M. N., Klunder A. D., Hayashi K. M., Protas H., Kepe V., Miller K. J., Huang S. C., Barrio J. R., Ercoli L. M., Siddarth P., Satyamurthy N., Liu J., Toga A. W., Bookheimer S. Y., Small G. W., Thompson P. M., *Neurobiol. Aging*, in press.
- 18) Kung M. P., Hou C., Zhuang Z. P., Zhang B., Skovronsky D., Trojanowski J. Q., Lee V. M., Kung H. F., *Brain Res.*, **956**, 202—210 (2002).
- 19) Zhuang Z. P., Kung M. P., Wilson A., Lee C. W., Plossl K., Hou C., Holtzman D. M., Kung H. F., *J. Med. Chem.*, **46**, 237—243 (2003).
- 20) Kung M. P., Hou C., Zhuang Z. P., Cross A. J., Maier D. L., Kung H. F., *Eur. J. Nucl. Med. Mol. Imaging*, **31**, 1136—1145 (2004).
- 21) Newberg A. B., Wintering N. A., Plossl K., Hochold J., Stabin M. G., Watson M., Skovronsky D., Clark C. M., Kung M. P., Kung H. F., *J. Nucl. Med.*, **47**, 748—754 (2006).
- 22) Kung H. F., Lee C. W., Zhuang Z. P., Kung M. P., Hou C., Plossl K., *J. Am. Chem. Soc.*, **123**, 12740—12741 (2001).
- 23) Chishti M. A., Yang D. S., Janus C., Phinney A. L., Horne P., Pearson J., Strome R., Zuker N., Loukides J., French J., Turner S., Lozza G., Grilli M., Kunicki S., Morrisette C., Paquette J., Gervais F., Bergeron C., Fraser P. E., Carlson G. A., George-Hyslop P. S., Westaway D., *J. Biol. Chem.*, **276**, 21562—21570 (2001).
- 24) Janus C., Chishti M. A., Westaway D., *Biochim. Biophys. Acta*, **1502**, 63—75 (2000).
- 25) Ono M., Kawashima H., Nonaka A., Kawai T., Haratake M., Mori H., Kung M. P., Kung H. F., Saji H., Nakayama M., *J. Med. Chem.*, **49**, 2725—2730 (2006).
- 26) Ono M., Kung M. P., Hou C., Kung H. F., *Nucl. Med. Biol.*, **29**, 633—642 (2002).
- 27) Gomez-Isla T., Price J. L., McKeel D. W., Jr., Morris J. C., Growdon J. H., Hyman B. T., *J. Neurosci.*, **16**, 4491—4500 (1996).
- 28) Haroutunian V., Perl D. P., Purohit D. P., Marin D., Khan K., Lantz M., Davis K. L., Mohs R. C., *Arch. Neurol.*, **55**, 1185—1191 (1998).
- 29) Price J. L., Morris J. C., *Ann. Neurol.*, **45**, 358—368 (1999).
- 30) Styren S. D., Hamilton R. L., Styren G. C., Klunk W. E., *J. Histochem. Cytochem.*, **48**, 1223—1232 (2000).
- 31) Dishino D. D., Welch M. J., Kilbourn M. R., Raichle M. E., *J. Nucl. Med.*, **24**, 1030—1038 (1983).
- 32) Price J. C., Klunk W. E., Lopresti B. J., Lu X., Hoge J. A., Ziolkowski K., Holt D. P., Meltzer C. C., DeKosky S. T., Mathis C. A., *J. Cereb. Blood Flow Metab.*, **25**, 1528—1547 (2005).
- 33) Lopresti B. J., Klunk W. E., Mathis C. A., Hoge J. A., Ziolkowski K., Lu X., Meltzer C. C., Schimmel K., Tsopeles N. D., DeKosky S. T., Price J. C., *J. Nucl. Med.*, **46**, 1959—1972 (2005).
- 34) Wang Y., Klunk W. E., Huang G. F., Debnath M. L., Holt D. P., Mathis C. A., *J. Mol. Neurosci.*, **19**, 11—16 (2002).
- 35) Ono K., Yoshiike Y., Takashima A., Hasegawa K., Naiki H., Yamada M., *J. Neurochem.*, **87**, 172—181 (2003).
- 36) Zhuang Z. P., Kung M. P., Hou C., Skovronsky D. M., Gur T. L., Plossl K., Trojanowski J. Q., Lee V. M., Kung H. F., *J. Med. Chem.*, **44**, 1905—1914 (2001).
- 37) Ono M., Yoshida N., Ishibashi K., Haratake M., Arano Y., Mori H., Nakayama M., *J. Med. Chem.*, **48**, 7253—7260 (2005).
- 38) Espeseth A. S., Xu M., Huang Q., Coburn C. A., Jones K. L., Ferrer M., Zuck P. D., Strulovici B., Price E. A., Wu G., Wolfe A. L., Lineberger J. E., Sardana M., Tugusheva K., Pietrak B. L., Crouthamel M. C., Lai M. T., Dodson E. C., Bazzo R., Shi X. P., Simon A. J., Li Y., Hazuda D. J., *J. Biol. Chem.*, **280**, 17792—17797 (2005).
- 39) Iwatsubo T., Odaka A., Suzuki N., Mizusawa H., Nukina N., Ihara Y., *Neuron*, **13**, 45—53 (1994).
- 40) Morris J. C., Storandt M., McKeel D. W. Jr., Rubin E. H., Price J. L., Grant E. A., Berg L., *Neurology*, **46**, 707—719 (1996).
- 41) Zhuang Z. P., Kung M. P., Hou C., Plossl K., Skovronsky D., Gur T. L., Trojanowski J. Q., Lee V. M., Kung H. F., *Nucl. Med. Biol.*, **28**, 887—894 (2001).
- 42) Ono M., Haratake M., Mori H., Nakayama M., *Bioorg. Med. Chem.*, **15**, 6802—6809 (2007).
- 43) Ono M., Hori M., Haratake M., Tomiyama T., Mori H., Nakayama M., *Bioorg. Med. Chem.*, **15**, 6388—6396 (2007).
- 44) Ono K., Hasegawa K., Naiki H., Yamada M., *J. Neurosci. Res.*, **75**, 742—750 (2004).
- 45) Yang F., Lim G. P., Begum A. N., Ubeda O. J., Simmons M. R., Ambegaokar S. S., Chen P. P., Kaye R., Glabe C. G., Frautschi S. A., Cole G. M., *J. Biol. Chem.*, **280**, 5892—5901 (2005).
- 46) Ryu E. K., Choe Y. S., Lee K. H., Choi Y., Kim B. T., *J. Med. Chem.*, **49**, 6111—6119 (2006).
- 47) Ono M., Maya Y., Haratake M., Ito K., Mori H., Nakayama M., *Biochem. Biophys. Res. Commun.*, **361**, 116—121 (2007).
- 48) Maya Y., Ono M., Watanabe H., Haratake M., Saji H., Nakayama M., *Bioconjug. Chem.*, **20**, 95—101 (2009).
- 49) Roberts M. J., Bentley M. D., Harris J. M., *Adv. Drug. Deliv. Rev.*, **54**, 459—476 (2002).
- 50) Harris J. M., Chess R. B., *Nat. Rev. Drug. Discov.*, **2**, 214—221 (2003).
- 51) Kung M. P., Hou C., Zhuang Z. P., Skovronsky D., Kung H. F., *Brain Res.*, **1025**, 98—105 (2004).
- 52) Zhang W., Oya S., Kung M. P., Hou C., Maier D. L., Kung H. F., *J. Med. Chem.*, **48**, 5980—5988 (2005).